DHAVAL RAMESHKUMAR SAJNANI

# Fatigue Life Enhancement of Metallic Aircraft Structures Using Bonded Crack Retarders: A Finite Element Study with VCCT and Cohesive Surface in ABAQUS

Dr. Wenli Liu
Aerospace Vehicle Design

MSc
Academic Year: 2024 - 2025

Supervisor: Dr. Wenli Liu
August 2025

Dr. Wenli Liu
Aerospace Vehicle Design

MSc

Academic Year 2024 - 2025

DHAVAL RAMESHKUMAR SAJNANI

# Fatigue Life Enhancement of Metallic Aircraft Structures Using Bonded Crack Retarders: A Finite Element Study with VCCT and Cohesive Surface in ABAQUS

Supervisor: Dr. Wenli Liu
August 2025

This thesis is submitted in partial fulfilment of the requirements for the degree of Aerospace Vehicle Design
**(NB. Remove if the degree award is based solely on examination of the thesis)**

© Cranfield University 2025. All rights reserved. No part of this publication may be reproduced without the written permission of the copyright owner.
**(NB. Refer to the guidance in Chapter 1 if sponsored by the MOD or other employers/funders)**

## Academic integrity declaration

I declare that:

- The thesis submitted has been written by me alone.
- The thesis submitted has not been previously submitted to this university or any other.
- That all content, including primary and/or secondary data, is true to the best of my knowledge.
- That all quotations and references have been duly acknowledged according to the requirements of academic research.
- I understand that to knowingly submit work in violation of the above statement will be considered by examiners as academic misconduct.

# Fatigue Life Enhancement of Metallic Aircraft Structures Using Bonded Crack Retarders

## A Finite Element Study with VCCT and Cohesive Surface in ABAQUS

**Dhaval Rameshkumar Sajnani**

## I.ABSTRACT

This research investigates the fatigue life enhancement of aluminium structures through the application of bonded crack retarders, modelled and analysed using the finite element (FE) method in ABAQUS. The study focuses on an aluminium plate specimen with centrally located cracks, reinforced symmetrically on both surfaces by bonded crack retarders, aiming to delay crack propagation and extend structural service life. The FE model incorporates advanced fracture mechanics techniques, including the Virtual Crack Closure Technique (VCCT) and the Cohesive Surface, to accurately simulate crack initiation and growth under cyclic loading. From these simulations, the strain energy release rate (SERR) components are extracted and utilised to compute stress intensity factors (SIFs). These SIF values form the basis for fatigue life prediction, performed both through AFGROW simulations. The computational results are rigorously compared against previously conducted experimental data to assess model fidelity and predictive accuracy. The outcomes of this study contribute to the understanding of bonded crack retarder performance and provide a validated numerical framework for fatigue life estimation in aerospace grade aluminium components.

**Keywords:**

Fatigue analysis, FEA, ABAQUS, VCCT, CZM, Crack Propagation, Damage Tolerance

# II.NOMENCLATURE

| | |
|---|---|
| VCCT | Virtual Crack Closure Technique |
| CZM | Cohesive Zone Modelling |
| SIF | Stress Intensity Factor |
| SERR | Strain Energy Release Rate |
| IAS | Integral Aircraft Structures |
| BCR | Bonded Crack Retarders |
| GLARE | Glass Laminate Aluminium Reinforced Epoxy |
| FE | Finite element |
| BK | Benzeggagh–Kenane |
| LEFM | Linear elastic fracture mechanics |
| ENRTT11 | Energy Release Rate for Mode I |

## A. Symbols

| | |
|---|---|
| K | Stress Intensity Factor |
| G | Strain Energy Release Rate |
| β | Stress Intensity Correction Factor |
| $\sigma_n$ | Normal stress |
| $\sigma_{n0}$ | Limit Normal Stress |
| $\tau_s$ | Shear stress in the first direction |
| $\tau_{s0}$ | Limit Shear stress in the first direction |
| $\tau_t$ | Shear stress in the transverse direction |
| $\sigma\tau_{t0}$ | Limit Shear stress in the transverse direction |
| $\eta$ | Mode interaction parameter |
| Gc | Mixed-mode critical energy release rate |
| E | Youngs Modulus |
| E′ | Effective Modulus |
| ν | Poisson's ratio |
| $\sigma_Y$ | Yield strength. |
| a | Crack length |
| N | Number of Fatigue cycles |
| C, n, p | Material constants |
| ΔK | Stress intensity factor range ($K_{max}$–$K_{min}$) |
| $K_{max}$ | Maximum stress intensity factor |
| Kc | Fracture toughness |
| $\Delta K_{th}$ | Threshold Stress intensity factor range |
| F(R) | Empirical factor accounting for load ratio effects ($R=\sigma_{min}/\sigma_{max}$) |
| $\eta_I$, $\eta_{II}$, $\eta_{III}$ | Mode-specific interaction parameters |
| $G_I$, $G_{II}$ and $G_{III}$ | Mode I, II, and III energy release rates |
| $G_{IC}$, $G_{IIC}$ and $G_{IIIC}$ | Mode I, II, and III energy release rates critical values |

# 1.0 Introduction

Integral Aircraft Structures (IAS) have become increasingly prevalent in modern airframe design due to their contribution to structural weight reduction, improved aerodynamics, and manufacturing efficiency. Unlike traditional built-up assemblies where skin panels are mechanically fastened to stiffeners, IAS are machined or formed from a single piece of material, integrating both skin and stiffening elements. This approach reduces part count, minimises fastener-induced stress concentrations, and can offer significant fuel efficiency benefits through weight savings. However, the monolithic nature of IAS results in reduced damage tolerance when compared with conventional built-up structures, as the absence of discrete joints eliminates natural crack arrest locations. Once initiated, cracks in IAS can propagate rapidly, which poses challenges for maintaining residual strength and fatigue life, especially under the rigorous load spectra experienced by aircraft in service.

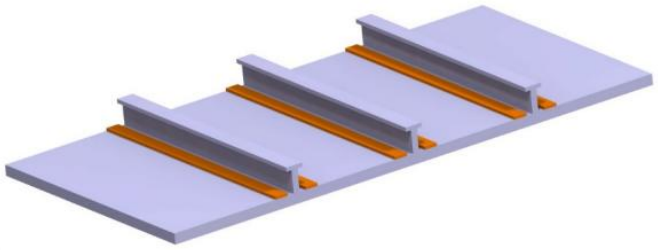

**Figure 1: Integrated Aircraft Structures (IAS) with Bonded Crack Retarders (BCR)**

To address these limitations, selective reinforcement strategies have been developed, one of the most promising being the application of Bonded Crack Retarders (BCRs). These are thin, high-strength material straps adhesively bonded to the surface of an IAS panel in locations prone to crack growth. Early applications date back to the 1970s, when such bonded reinforcements were initially employed as patch repairs for metallic skins. Subsequent research demonstrated that BCRs, when integrated during manufacturing, could significantly enhance damage tolerance by reducing crack growth rates and delaying the attainment of critical crack lengths. In recent years, fibre-metal laminates such as GLARE (Glass Laminate Aluminium Reinforced Epoxy) have been increasingly used as BCR material. GLARE offers a unique combination of aluminium's metallic toughness and glass-fibre composite's fatigue resistance, providing superior crack bridging capability and excellent corrosion resistance. Experimental studies have shown that GLARE BCRs can substantially extend fatigue life by redistributing stresses around the crack tip, reducing the effective stress intensity factor range.

In this study, an Aluminium 2624-T351 panel is reinforced on both surfaces with double-side GLARE BCRs, bonded using FM94 aerospace-grade adhesive. The reinforcement configuration is chosen to maximise crack-bridging effects on both crack faces, thereby increasing fatigue crack propagation life.

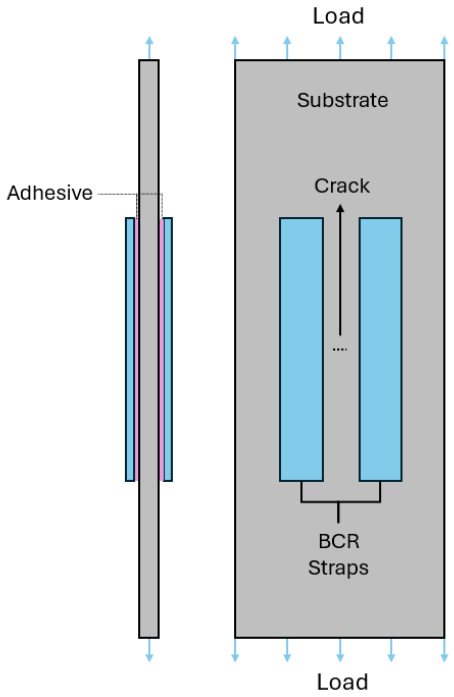


**Figure 2: Aluminium Specimen with BCR**

A finely meshed finite element (FE) model is developed in ABAQUS, employing symmetry about the X-axis to reduce computational demand by modelling only half of the panel. Fatigue crack growth is simulated using the Virtual Crack Closure Technique (VCCT), which is grounded in linear elastic fracture mechanics and computes the strain energy release rate by equating the energy required to close the crack with that released during extension.

Complementing VCCT, the Cohesive Zone Method (CZM) is also implemented to capture interfacial fracture at the BCR-substrate bond line. This approach models fracture as a gradual process governed by a traction–separation law, allowing simulation of both damage initiation and evolution. In the present FE model, cohesive behaviour is defined through a surface-to-surface contact interaction with cohesive properties assigned to replicate adhesive failure characteristics.

At predefined crack lengths, incremented in steps of 5 mm, the model extracts Strain Energy Release Rate (SERR) components. From these, stress intensity factor ranges are derived, enabling fatigue life estimation using AFGROW. The predicted fatigue cycles to failure for the GLARE-reinforced configuration are compared directly with available experimental data [3], providing a quantitative assessment of model fidelity and the degree of fatigue life enhancement attributable to the double-side GLARE BCRs.

# 2.0 Finite Element Modelling

## 2.1 Introduction to finite element modelling in fracture mechanics

The finite element (FE) analysis for this study was conducted using ABAQUS 2024 [8], a general-purpose finite element software widely adopted in the aerospace industry for structural analysis. The primary objective was to replicate the geometry, material configuration, loading, and boundary conditions from experimentally tested specimens, thereby enabling direct comparison of numerical predictions against physical test results [1][3]. The model represented an aluminium alloy substrate reinforced with double-sided bonded crack retarders (BCRs) manufactured from GLARE, bonded using FM94 epoxy film adhesive.

The FE modelling approach was designed to:

- Accurately capture the stress intensity factor (SIF) and strain energy release rate (SERR) at the crack front for different crack lengths.
- Incorporate realistic material properties and interface definitions to simulate adhesive bonding and potential disbond behaviour.
- Replicate experimental load application and constraints to achieve high fidelity between simulation and test.

The analysis was performed under Linear Elastic Fracture Mechanics (LEFM) assumptions [10][11][13], given that the plastic zone around the crack tip was small compared to the crack size. The model geometry exploited symmetry along the longitudinal axis (X-axis), enabling simulation of only half of the plate while doubling the results to represent the full specimen. This symmetry assumption reduced computational cost while maintaining accuracy in the stress field distribution [8].

## 2.2 Geometry and modelling rationale

The geometry modelled in ABAQUS followed the experimental middle tension (M(T)) specimen configuration described in ASTM E647 [20], enabling direct validation against physical test results [1][3]. The substrate was aluminium alloy 2624-T351 with a total length of 400 mm and a width of 140 mm. A central through-thickness crack of 20 mm was introduced perpendicular to the loading axis.

Double-sided bonded crack retarders (BCRs) were positioned symmetrically on both sides of the substrate to minimise secondary bending effects. Each strap measured 180 mm in length and 26 mm in width.

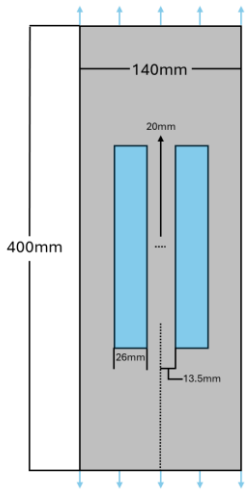


**Figure 3: Aluminium Specimen with BCR Geometry**

The model was constructed using X-symmetry in ABAQUS, with only half of the specimen represented in the finite element domain. This symmetry approach significantly reduced computational cost while maintaining accuracy in the predicted stress intensity and strain energy release rate distributions.

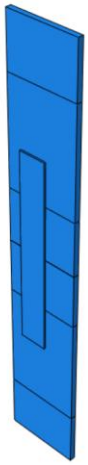

**Figure 4: ABAQUS Model with X-symmetry**

## 2.3 Materials

### 2.3.1 Aluminium 2624-T351 (Substrate)

The substrate in the FE model was an aluminium alloy 2624-T351, selected for its established use in aerospace structural applications and availability of experimental data for comparison. Aluminium 2624-T351 is a high-strength, heat-treated alloy with good fracture toughness and fatigue performance, often used in wing skins and fuselage panels where crack growth resistance is critical. The mechanical properties employed in the model are given in Table 1, consistent with values reported in MMPDS and validated against available experimental datasets [4].

**Table 1: Aluminium 2624-T351 properties [a)]**

| Property | Value | Unit |
|---|---|---|
| **Young's modulus, E** | 71 | GPa |
| **Poisson's ratio, ν** | 0.33 | – |

a) Taken from Ref. [4]

**Note** – Values for the $G_{IC}$, $G_{IIC}$ and $G_{IIIC}$ adopted in this study were considered to be artificially elevated. This approach was necessary to prevent premature static failure of the specimen during simulation, as the primary objective was not to directly validate fracture toughness but rather to extract accurate β-values corresponding to different crack lengths. These β-values can subsequently be used as inputs in AFGROW for fatigue life prediction. Furthermore, reliable experimental fracture toughness data for aluminium alloy 2624-T351 are not readily available in the open literature, making this strategy both practical and justified for the intended purpose of the analysis.

### 2.3.2 GLARE 2A 6/5 (Straps)

The bonded crack retarders (BCRs) were modelled as GLARE 2A 6/5 straps, a fibre–metal laminate consisting of alternating layers of 2024-T3 aluminium and unidirectional glass–epoxy prepreg. In this configuration, the "2A" refers to the GLARE grade, and "6/5" indicates the lay-up sequence of six aluminium layers and five glass fibre–epoxy layers. GLARE exhibits high fatigue resistance, damage tolerance, and corrosion resistance, with a coefficient of thermal expansion closer to aluminium than to carbon fibre composites, reducing thermal residual stresses [5][6].

Consistent with established practice in fibre, metal laminate structural modelling, the GLARE strap was represented as a single equivalent plate with homogenised stiffness so that global load sharing and crack-bridging effects were captured without ply-by-ply modelling [5][6][7]. This approach preserves the correct in-plane stiffness and overall bending response for crack-retardation studies while avoiding the large element counts and numerous ply-level interfaces that would otherwise be required. Table 2 lists the equivalent properties used.

**Table 2: Equivalent properties for GLARE 2A 6/5** [a)]

| Property | Value | Unit |
|---|---|---|
| **Young's modulus, E** | 66.5 | GPa |
| **Poisson's ratio, ν** | 0.33 | – |

a) Taken from Ref. [2]

### 2.3.3 FM94 (Adhesive)

The adhesive used to bond the GLARE straps to the aluminium substrate was FM94, a film adhesive widely used in aerospace applications for its high fracture toughness and durability. The values adopted in the model are consistent with those obtained from experimental characterisation tests, such as those performed by Doucet [1], which measured Mode I, II, and III fracture energies and nominal cohesive strengths for bonded Aluminium–GLARE joints.

## 2.4 Meshing strategy and element choice

Continuum shell elements (SC8R in ABAQUS) were selected for both the substrate and the straps. These elements provide the computational efficiency of shell formulations while retaining the capability to capture through-thickness stress distributions, making them well-suited for layered metallic–composite hybrid structures. In the present case of double-sided straps, continuum shells also ensured that any out-of-plane bending effects, which are significant in asymmetric single-strap configurations, remained minimal and accurately represented. Furthermore, SC8R elements avoid shear-locking issues in thin structures and enable accurate prediction of fracture parameters such as the strain energy release rate (SERR) in VCCT analyses [8].

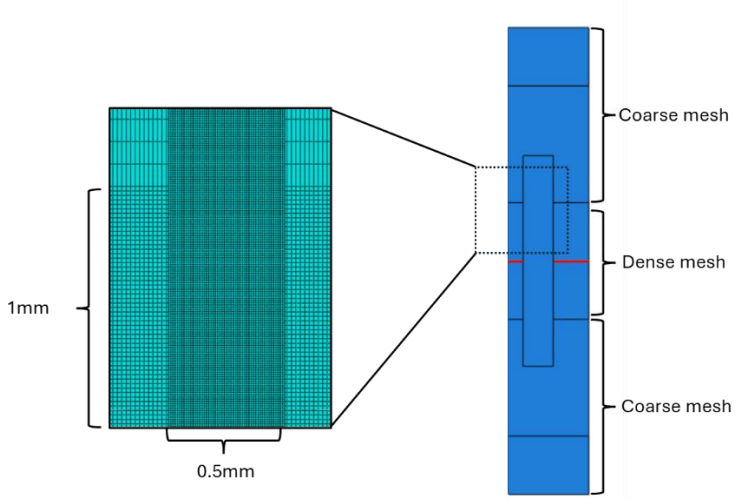


**Figure 5: Mesh Structure**

A local refinement was applied in the vicinity of the crack front. The substrate mesh was refined to 1 mm element size around the crack tip, with coarse mesh away from the densely meshed region to manage element counts within academic licence limits. The straps were meshed to 0.5 mm in the bonded region to resolve adhesive shear and peel stresses. This gradation follows standard mesh-convergence principles in fracture mechanics, concentrating refinement where SERR extraction is most sensitive to discretisation [9][10][11][12]. Figure 5 illustrates the refinement around the crack tip.

### 2.5 Crack-tip interaction (VCCT)

The Virtual Crack Closure Technique (VCCT) is a widely used numerical method for determining the strain energy release rate (SERR) at the crack tip in finite element (FE) simulations. It is based on Irwin's crack closure integral concept, which states that the energy released during a small crack extension is equal to the work required to close the crack by the same amount [13]. The original finite element formulation of VCCT was introduced by Rybicki and Kanninen [14] and has since been refined for greater numerical accuracy and stability.

In its standard form, VCCT determines the mode-dependent SERR components, Mode I (opening), Mode II (sliding), and Mode III (tearing) by computing nodal forces ahead of the crack tip and relative displacements behind it. These quantities are extracted from a single FE analysis without requiring mesh remeshing or re-analysis, making VCCT both computationally efficient and robust [15]. The formulation assumes that crack extension is small enough that the stress and displacement fields at the crack tip remain representative over the small propagation length, ensuring accurate energy calculations.

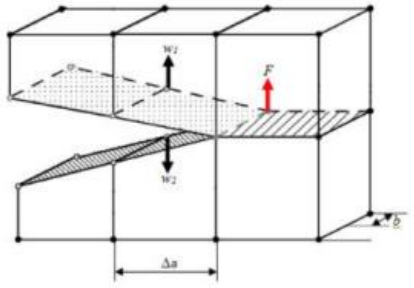


**Figure 6: VCCT for 8 nodes continuum shell elements (SC8R) – Through thickness view**

Within ABAQUS, VCCT is implemented using surface-based interactions or contact definitions at the crack interface. The crack front is discretised into pairs of opposing nodes across the interface, with the crack growth direction predefined. At each analysis increment, ABAQUS calculates the SERR values for each mode using the nodal forces and displacements and compares them to user-specified critical fracture energies, $G_{IC}$, $G_{IIC}$ and $G_{IIIC}$ [8]. Crack advance occurs in the analysis when the calculated SERR for any mode reaches or exceeds its corresponding critical value, simulating fracture propagation in a physically realistic manner.

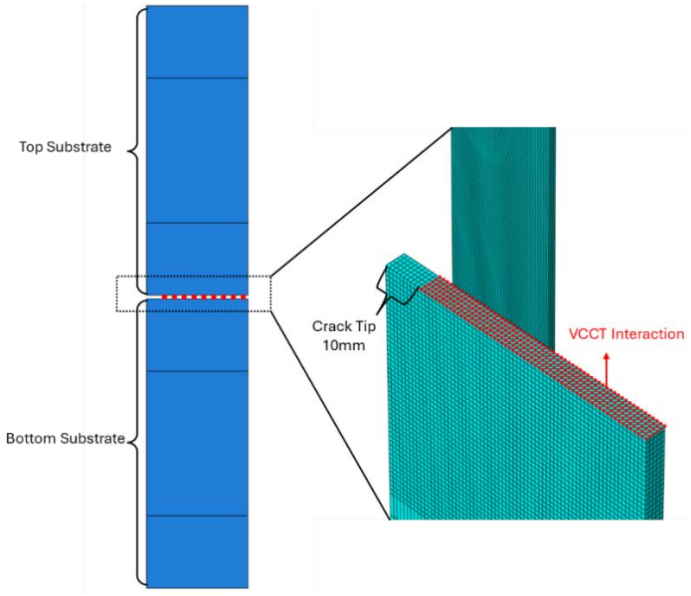


**Figure 7: Crack tip interaction**

In the present work, VCCT was implemented in ABAQUS [8] by defining a contact interaction between the upper and lower halves of the substrate along the predefined crack plane. This interaction included a fracture criterion based on the Benzeggagh–Kenane mixed-mode law (see Section 2.7), with the Mode I, II, and III fracture toughness values ($G_{IC}$, $G_{IIC}$ and $G_{IIIC}$ ) defined to be artificially elevated to prevent premature static failure of the specimen during simulation. The crack growth direction was fixed along the predefined symmetry plane, and no re-meshing was required between increments. Instead, the crack length was increased in discrete steps of 5 mm by updating the bonded region through the limit bonding feature manually in ABAQUS, allowing direct extraction of SERR values for each crack length increment, see Figure 8.

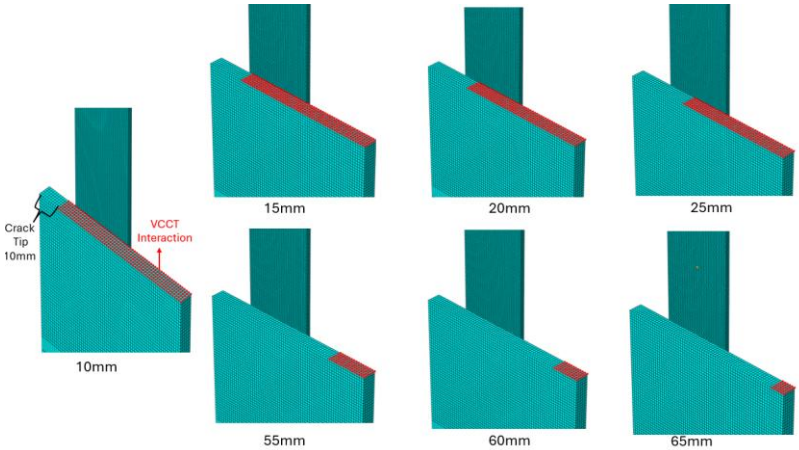


**Figure 8: Crack tip interaction at different crack lengths**

### 2.6 Substrate-BCR interaction (CZM/ Cohesive Surface)

Cohesive zone modelling represents the fracture process zone by a traction, separation relationship, in which the interface responds elastically up to a damage initiation criterion and then degrades according to a damage evolution law until complete decohesion [16][17].

Abaqus offers cohesive elements and surface-based cohesive behaviour. Surface-based cohesive interaction was used here, because it reduces mesh complexity, is compatible with arbitrary bonded footprints, and integrates well with a VCCT crack interface in the same model.

Damage initiation used the quadratic nominal stress criterion and damage evolution was energy-based with mixed-mode interaction governed by a traction, separation law, discussed below in Section 2.7. This arrangement allowed adhesive failure at the strap, substrate interface to initiate and grow when the local stress state and energy release met the calibrated conditions. The failure criterion equation in mechanics of materials, often used in cohesive zone modelling (CZM) or adhesive joint failure is given as.

$$\left(\frac{\sigma_n}{\sigma_{n0}}\right)^2 + \left(\frac{\tau_s}{\tau_{s0}}\right)^2 + \left(\frac{\tau_t}{\sigma\tau_{t0}}\right)^2 = 1 \qquad (1)$$

Where,

$\sigma_n$ = normal stress
$\tau_s$= shear stress in the first direction
$\tau_t$ = shear stress in the transverse direction
$\sigma_{n0}, \tau_{s0}, \sigma\tau_{t0}$ = corresponding strength limits

Doucet [1] reported that adhesive separation in bonded crack retarders tended to initiate at, or near, the substrate crack plane and then evolve in a triangular planform under fatigue loading, with the apex near the crack and the base extending towards the strap ends. This shape reflects the coupled peel and shear stress distribution in the bond line. Peel tends to peak near geometric discontinuities where curvature or bending induces opening, while shear accumulates towards the free edges where the load transfer between strap and substrate is the largest. As the number of cycles increases, the disbond region widens and advances along the load path, giving a triangular footprint that has been observed and reproduced numerically in bonded repair and crack-retarder literature.

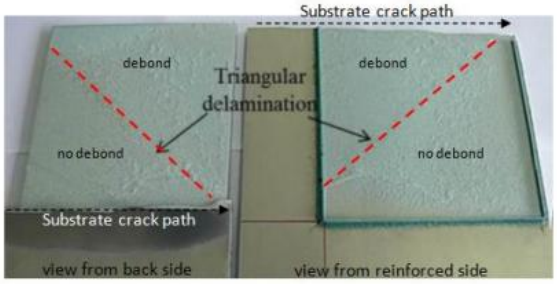


(Debond is triangular in shape and covers almost half of the reinforced area as shown in the schematic representation below)

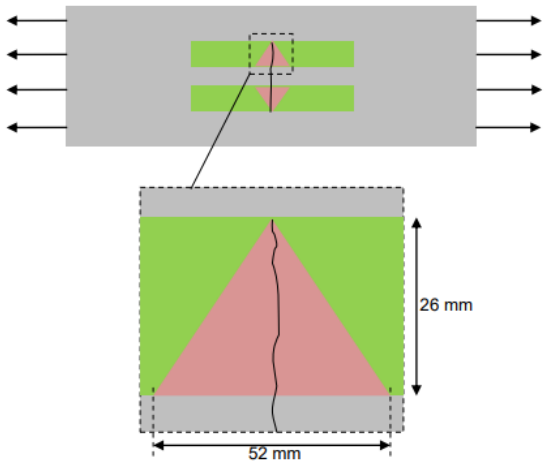


**Figure 9: Triangular Disbond Explained as per Doucet, Ref. [1]**

This behaviour was reproduced in the present finite element model by manually drafting the disbond in a triangular pattern and releasing nodes progressively. Practically, the bonded footprint between strap and substrate was partitioned into a series of node sets along the strap length and width, pre-defining the triangular front. In each static step, corresponding to a 5 mm increase in crack length, the next node set within the triangular region was released using the limit bonding option in the interaction definition, which converts selected contact pairs from bonded to unbonded. This produced a widening disbond front consistent with Doucet's observations, while keeping the mesh intact, preserving element quality, and avoiding the need for element deletion or complex cohesive element damage algorithms. The approach allowed the adhesive failure to be applied deterministically so that its interaction with the crack-tip SERR could be quantified at each discrete state. Figure 9 sketches the triangular disbond concept reported experimentally, while Figure 10 shows the implemented node-set sequence used to realise this front in the model.

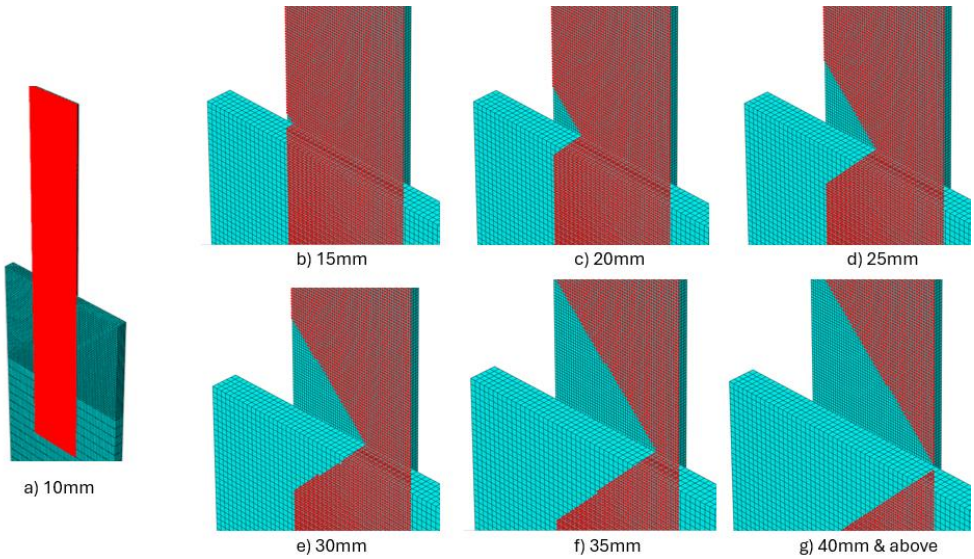


**Figure 10: Manual triangular disbond with varying crack lengths (Nodes Released)**

### 2.7 Traction/Separation laws

Mixed-mode interaction defines how the mode components of fracture energy combine to trigger growth. Three commonly used laws were considered.

#### 2.7.1 Power Law

The power law criterion assumes that the total energy release rate, $G_T$ is a weighted combination of the individual mode contributions, each normalised by its critical value:

$$\left(\frac{G_I}{G_{IC}}\right)^{\eta} + \left(\frac{G_{II}}{G_{IIC}}\right)^{\eta} + \left(\frac{G_{III}}{G_{IIIC}}\right)^{\eta} = 1 \quad (2)$$

Where,

$G_I$, $G_{II}$ and $G_{III}$ = Mode I, II, and III energy release rates
$G_{IC}$, $G_{IIC}$ and $G_{IIIC}$ = Mode I, II, and III energy release rates critical values
$\eta$ = mode interaction parameter [16]

Advantages: Simple to implement, requires minimal experimental characterisation, and can be applied in both 2D and 3D fracture problems.

Limitations: Does not capture the experimentally observed increase in fracture resistance under mixed-mode conditions, particularly in bonded joints and fibre–metal laminates.

#### 2.7.2 Reeder's Law

Reeder's law is a three-dimensional mixed-mode criterion that introduces separate exponents for each fracture mode and explicitly incorporates Mode III effects:

$$\left(\frac{G_I}{G_{IC}}\right)^{\eta_I} + \left(\frac{G_{II}}{G_{IIC}}\right)^{\eta_{II}} + \left(\frac{G_{III}}{G_{IIIC}}\right)^{\eta_{III}} = 1 \quad (3)$$

Where

$\eta_I$, $\eta_{II}$, $\eta_{III}$ are mode-specific interaction parameters [19].

Advantages: Greater flexibility for fitting experimental data in 3D loading conditions; capable of capturing complex mode-mix effects.

Limitations: Requires extensive and separate experimental determination of the parameters for each mode, making it less practical for cases with limited data.

#### 2.7.3 Benzeggagh–Kenane (BK) Law

The BK law improves on the power law by introducing a mode-mixity-dependent fracture toughness for shear modes:

$$G_C = G_{IC} + (G_{IIC} - G_{IC})\left(\frac{G_s}{G_I + G_s}\right)^{\eta} \quad (4)$$

Where

$Gs$ = $G_{II}$ + $G_{III}$, Gc = mixed-mode critical energy release rate
$\eta$ is obtained experimentally [18]

Advantages: Matches mixed-mode fracture behaviour observed in adhesively bonded joints and fibre–metal laminates more accurately than the power law, particularly in cases with significant Mode II contributions.

The bonded crack retarder configuration leads to a significant contribution from shear modes due to load transfer through the adhesive layer. Hence, The BK law's ability to capture mode-dependent toughness variation makes it more representative of the physical fracture process in this application.

### 2.8 Step definition, Loads and boundary conditions

Rather than a single direct fatigue step, the analysis used a sequence of static general steps, each representing a specific crack length and disbond footprint: 10, 15, 20, …, up to 69 mm. This strategy delivered several advantages. First, it allowed direct extraction of mode-separated SERR at each crack length without post-hoc interpolation. Second, it avoided use of complex user subroutines or extensive Python automation to manage continuous crack advance. Third, it reduced runtime relative to full cycle-by-cycle modelling, while improving numerical stability because each step was short, with well-controlled contact status changes. Finally, it aligned directly with the planned life calculations, which use SERR, or SIF, at discrete crack sizes.

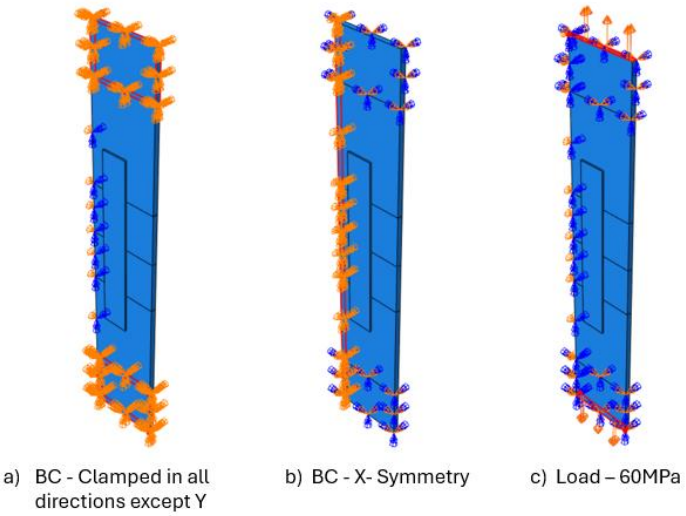


**Figure 11: Boundary Conditions (BC) and Load definition**

To replicate the experimental test arrangement, a nominal 60 MPa remote tensile stress was applied to the specimen ends. The first 50 mm at each end was constrained to emulate universal testing machine grips, with motion allowed only in the axial, Y, direction. Along the longitudinal mid-plane, X symmetry was enforced so that only half of the physical panel was modelled, halving computational cost while preserving the full structural response.

# 3.0 Fatigue Life Calculation

## 3.1 Obtaining Mode I Strain Energy Release Rate from FE Analysis

The first step in the fatigue life calculation was to determine the Mode I strain energy release rate ($G_I$) for each prescribed crack length from the finite element (FE) simulations. This parameter quantifies the energy available for crack extension per unit of newly created fracture surface and is fundamental in Linear Elastic Fracture Mechanics (LEFM) [10][12].

In this work, the Virtual Crack Closure Technique (VCCT) was employed to evaluate $G_I$ at the crack front. VCCT is based on the principle that the work required to close a crack by a small extension is equivalent to the energy released if the crack extends by the same amount [15]. Within Abaqus, the output variable ENRTT11 corresponds to the mode-I nodal energy release rate at the crack tip, computed over the crack front in accordance with the VCCT formulation [8][21].

As the present work focuses solely on double-sided bonded crack retarders (BCRs), $G_I$ was taken from a single surface of the specimen. In symmetric reinforcement configurations, the load path through the thickness is balanced, which suppresses the secondary bending effects that would otherwise cause face-to-face variation in $G_I$ [23][2][3].

The resulting $G_I$ (a) data formed the foundation for the subsequent steps in the fatigue life prediction process, enabling calculation of the corresponding stress intensity factor ($K_I$) and geometry correction factor β(a) for each crack length.

## 3.2 Conversion of SERR (G) to SIF (K)

Once the mode-I strain energy release rate $G_I$ values had been obtained from the FE model for each crack length 'a', the corresponding mode-I stress intensity factors ($K_I$) were determined using the classical LEFM relationship [10][12]:

$$K_I(a) = \sqrt{E'.G_I(a)} \tag{5}$$

where E′ is the effective modulus and depends on the stress state at the crack tip:

$$E' = \begin{cases} E & \text{for plane Stress} \\ \dfrac{E}{1-\upsilon^2} & \text{for plane Strain} \end{cases} \tag{6}$$

Here, E is the Young's modulus and ν is the Poisson's ratio of the substrate material. This relationship arises from Irwin's formulation linking energy release rates to stress intensity factors in isotropic, linear-elastic materials [13].

The distinction between plane stress and plane strain is critical in fracture analysis.

**Plane Stress** occurs when the specimen is thin relative to the crack-front plastic zone, and out-of-plane stresses (σz) are negligible. The material is free to contract or expand in the thickness direction. This condition is typical for thin skins or panels in aerospace structures [10][12][24].

**Plane Strain** occurs when the specimen is sufficiently thick such that deformation in the thickness direction is restrained (εz=0), leading to triaxial constraint and a smaller plastic zone size. Plane strain conditions generally produce higher apparent fracture toughness ($K_{IC}$) and are typical in thick plates or near the mid-thickness of large components [10][12].

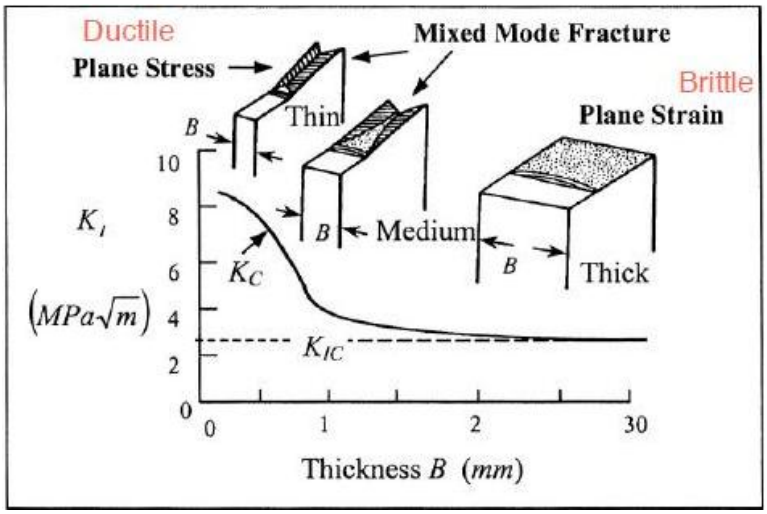


**Figure 12: Effect of Specimen thickness on $K_C$ (Fracture Toughness)**

A practical criterion for ensuring plane strain at the crack tip, as per ASTM E399, is [24]:

$$B, a, (W - a) \geq 2.5 \left(\frac{K_{IC}}{\sigma_Y}\right)^2 \tag{7}$$

Where

B = Specimen thickness
W = Specimen width
$\sigma_Y$ = Specimen Yield strength.

In this study, the specimens reinforced with double-sided GLARE straps had an aluminium substrate thickness that did not meet the above requirement for plane strain. Combined with the relatively low applied stress level and the geometry of the M(T) configuration, this means that plane stress dominates at the crack tip. Accordingly, the effective modulus was taken as E′=E in all calculations. This is consistent with previous experimental observations on similar thin aluminium panels [23][3].

### 3.3 Determination of β(a)

With $K_I$ (a) determined, the geometry correction factor β(a) was calculated for each crack length according to [10][12]:

$$\beta(a) = \frac{k_I(a)}{\sigma\sqrt{\pi a}} \tag{8}$$

Here, σ is the nominal far-field stress in the specimen, evaluated from the applied load and net section geometry. For the constant-amplitude loading used in this study, σ remains fixed for all crack lengths.

The β(a) factor encapsulates the influence of specimen geometry, loading configuration, and the presence of the bonded reinforcements. For double-sided BCRs, β(a) reflects not only the M(T) baseline geometry but also the stiffness and load sharing provided by the straps [2][3][23].

The calculated β(a) values were tabulated for the full range of crack lengths analysed. This β(a) table serves as the principal input for AFGROW analysis.

### 3.4 Life Prediction in AFGROW using β(a)

AFGROW (Air Force Growth) is a widely used fracture mechanics tool developed by the United States Air Force for predicting crack growth under both constant- and variable-amplitude loading [25]. It supports multiple crack growth models, including the NASGRO equation, and allows for the use of user-defined geometry factors β(a) [26][25]. This capability makes it particularly well-suited to reinforced geometries such as bonded crack retarders (BCRs), where closed form β solutions are not available and must instead be derived from FE analysis [15].

In the present work, the β(a) values computed in Section 3.3 were tabulated and directly imported via AFGROW's "User Defined Geometry" option. This ensures that the crack growth predictions account for the altered load path and stiffness effects introduced by the double-sided straps.

#### 3.4.1 NASGRO Equation Formulation

The NASGRO equation is a semi-empirical crack growth law that generalises the Paris Law to include the effects of crack closure, load ratio, threshold behaviour, and fracture toughness limits [25]:

$$\frac{da}{dN} = C\left[\left(\frac{1-\frac{\Delta K_{\text{th}}}{\Delta K}}{1-\frac{K_{\max}}{Kc}}\right)^{p} \Delta K^{n}\right] F(R) \tag{9}$$

Where,

a = crack length
N = number of cycles
C, n, p = material constants determined experimentally
ΔK = stress intensity factor range ($K_{max}$−$K_{min}$)
Kmax = maximum stress intensity factor in the cycle
Kc = fracture toughness
$\Delta K_{th}$ = threshold stress intensity factor range for crack growth
F(R) = empirical factor accounting for load ratio effects ($R=\sigma_{min}/\sigma_{max}$)

Unlike the simpler Paris Law [10], NASGRO can model the complete crack growth curve:

- Near threshold region ($\Delta K \approx \Delta K_{th}$)
- Paris region (mid-growth rates where $da/dN \propto \Delta K^{n}$)
- Near fracture region ($K_{max} \rightarrow Kc$)

The inclusion of the fracture toughness term $(1 - K_{max}/K_c)^{-q}$ ensures that growth rates accelerate sharply as $K_{max}$ approaches $K_c$, capturing instability prior to final failure.

The alloy under consideration, AA2624-T351, has been characterised extensively for aerospace applications [3][23][27]. Material constants C, n, p, ΔKth, Kc were taken from published experimental fatigue crack growth data. These same material properties were used in both the FE model and AFGROW to maintain consistency and avoid artificially optimistic or pessimistic life estimates.

### 3.4.2 AFGROW Analysis Procedure

The AFGROW-based life calculation for each configuration followed these steps:

- Define material model – Input Al 2624-T351 properties
- Define load – Set constant-amplitude loading with $\sigma_{max}$ matching the FE model and R=0.1
- Import β(a) table – Load the user-defined β(a) curve covering the entire crack length range analysed.
- Select NASGRO model
- Integrate da/dN – Allow AFGROW to compute crack growth incrementally until failure criterion is reached (either $K_{max} \rightarrow K_c$ or net-section yield).

Using β(a) from FE directly in AFGROW has several advantages:

- Geometric accuracy – Accounts for reinforcement stiffness, load sharing, and any local perturbations due to adhesive and strap geometry.
- Material fidelity – Incorporates experimentally determined NASGRO parameters for the specific alloy.
- Full crack growth curve – Predicts life across threshold, Paris, and near-fracture regimes without artificial truncation at intermediate regions.

This method has been shown in prior BCR studies to produce reliable fatigue life estimates when combined with accurate β(a) input [1][3][15][25].

# 4.0 Results and Discussions

## 4.1 Validation – M(T) Specimen Non-Reinforced

To validate the finite element (FE) model and the associated methodology, a baseline centre-cracked plate configuration without bonded crack retarders (BCRs) was first analysed. Using the virtual crack closure technique (VCCT), the strain energy release rate (SERR) values were extracted from the Abaqus output database (ODB) files and subsequently processed to calculate the geometry correction factor (β).

The calculated β-values demonstrated the expected increase with crack length, consistent with fracture mechanics theory [10][12]. These data were subsequently used within AFGROW to predict fatigue life.

**Table 3: M(T) Specimen Non-Reinforced**

| a (m) | SERR (N/m) | β (SIFC) | ΔK (MPa√m) |
|---|---|---|---|
| **0.010** | 1982.00 | 1.1155 | 10.6764 |
| **0.015** | 3103.00 | 1.1396 | 13.3587 |
| **0.020** | 4350.00 | 1.1685 | 15.8167 |
| **0.025** | 5791.00 | 1.2059 | 18.2494 |
| **0.030** | 7528.00 | 1.2551 | 20.8071 |
| **0.035** | 9716.00 | 1.3201 | 23.6383 |
| **0.040** | 12610.00 | 1.4068 | 26.9296 |
| **0.045** | 16670.00 | 1.5250 | 30.9627 |
| **0.050** | 22820.00 | 1.6927 | 36.2268 |
| **0.055** | 33150.00 | 1.9452 | 43.6630 |
| **0.060** | 53850.00 | 2.3737 | 55.6499 |
| **0.065** | 114100.00 | 3.3196 | 81.0055 |

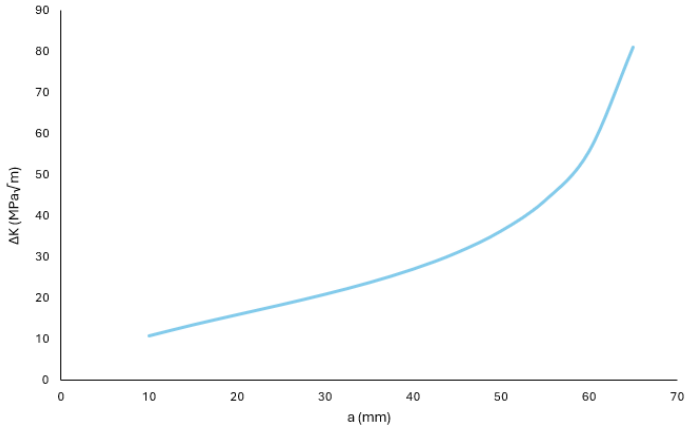


**Figure 13: ΔK for M(T) Specimen Non-Reinforced**

The predicted fatigue lives were then compared with published finite element and experimental results from prior Cranfield University studies [2][3][27]. Table 4 provides a comparison.

**Table 4: Fatigue Life Results for M(T) Specimen Non-Reinforced**

| Model | Fatigue Life | Method | Difference Percentage |
|---|---|---|---|
| **Dhaval 2025** | 103,100 | FEA | - |
| **Sudhakar 2017** | 100,380 | FEA | -2.6 |
| **Slater 2017** | 140,414 | Experimental | 26.6 |
| **Hill 2013** | 111,372 | Experimental | 7.4 |

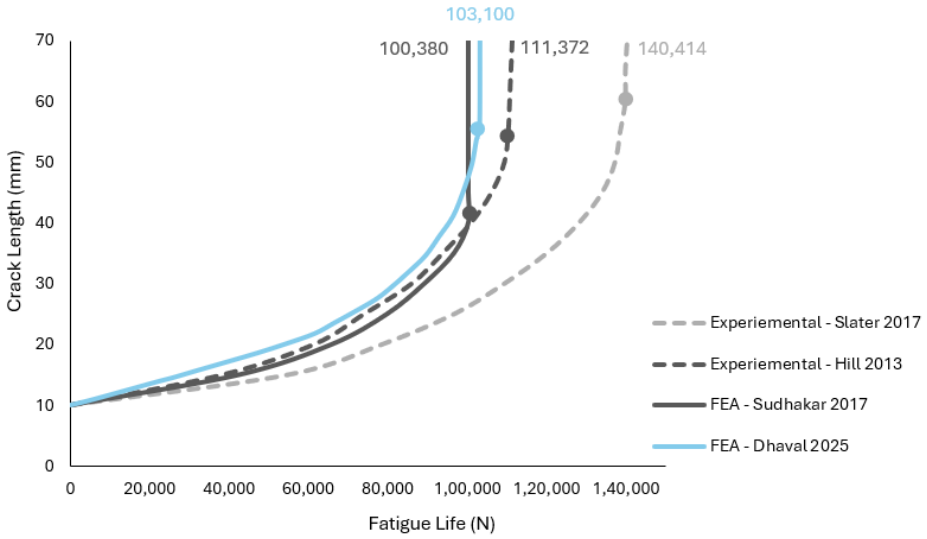


**Figure 14: Fatigue Life for M(T) Specimen Non-Reinforced**

The predicted fatigue life of 103,100 cycles from the current analysis shows good agreement with both Sudhakar's finite element results (100,380 cycles) and Hill's experimental values (111,372 cycles), with deviations within ~8%. While some scatter was observed when compared to Slater's experimental results (140,414 cycles), the predicted value remains conservative and within an acceptable range of variation, particularly given the sensitivity of experimental fatigue data to environmental and manufacturing effects such as room temperature, adhesive quality, and machining tolerances [28][30].

For AA2624-T351, the Mode-I plane-strain fracture toughness at room temperature has been experimentally determined to be approximately $K_{IC} \approx 53$ MPa$\sqrt{m}$, with corresponding yield strength $\sigma_{Ys} \approx 331$ MPa, UTS $\approx$ 434 MPa, and Young's modulus $E \approx 71$ GPa [31]. Using linear elastic fracture mechanics, this converts to a critical strain energy release rate of $G_{IC} \approx 35$–40 N/mm, depending on whether plane-strain or plane-stress conditions are assumed. In the present finite element analysis, the SERR values extracted from the VCCT procedure reached ~30 N/mm at a crack length of approximately 55 mm. This result lies just below the expected toughness range and, importantly, coincides with the onset of unstable crack growth observed experimentally in the 50–60 mm region of M(T) specimens, as reported by Slater and Hill [27][3].

The convergence of predicted and experimental data around the 50–60 mm crack length region provides strong evidence of model validity, since both numerical and physical tests identified this as the transition region into unstable crack growth.

Therefore, the baseline analysis confirmed that the FE methodology - incorporating VCCT, β-value extraction, and fatigue life prediction via AFGROW, produces results that are both conservative and consistent with experimental benchmarks. This establishes a sound foundation for extending the methodology to more complex reinforced cases with BCRs, where crack retardation and fatigue life enhancement can be quantified with confidence [30].

### 4.2 Double Side Symmetric BCRs

The principal case analysed in this study was the double-side symmetric BCR reinforced configuration, representing a realistic structural scenario. The reinforcement consisted of GLARE straps bonded symmetrically to both sides of the AA2624-T351 substrate with FM94 adhesive, replicating experimental test setups reported in the literature [1][3][23].

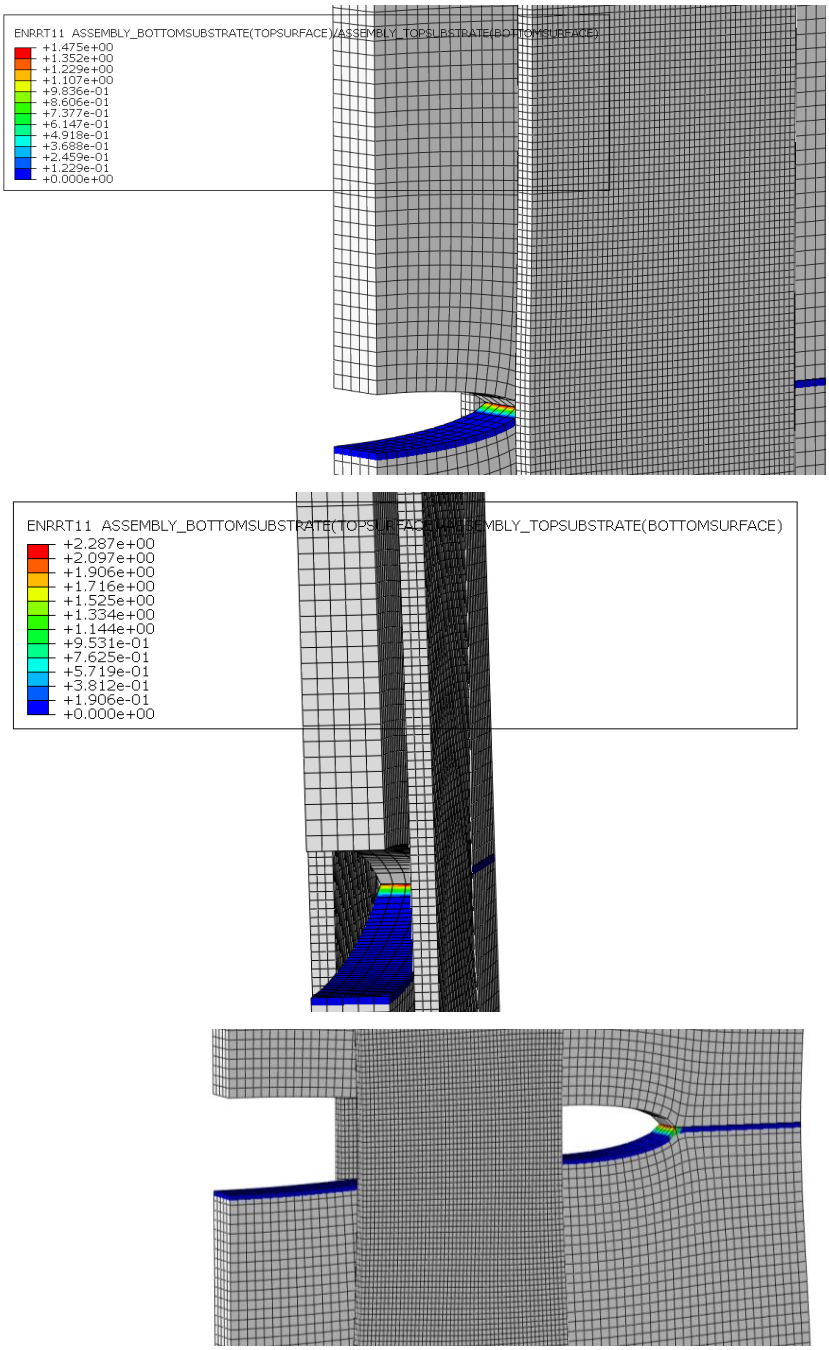


**Figure 15: ENRRT11 Results at different crack lengths (15mm, 40mm, 55mm)**

The strain energy release rate (SERR) values in Mode I were extracted from the FE model using VCCT. The corresponding β-values were obtained and subsequently used to calculate the stress intensity factor range (ΔK), which formed the basis for fatigue life prediction in AFGROW. These results are presented in Table 5.

**Table 5: Double Side Symmetric BCRs**

| a (m) | SERR (N/m) | β (SIFC) | ΔK (MPa√m) |
|---|---|---|---|
| **0.010** | 1121.00 | 0.8389 | 8.0292 |
| **0.015** | 1475.00 | 0.7857 | 9.2102 |
| **0.020** | 1512.00 | 0.6889 | 9.3250 |
| **0.025** | 1594.00 | 0.6327 | 9.5745 |
| **0.030** | 1723.00 | 0.6005 | 9.9544 |
| **0.035** | 1934.00 | 0.5890 | 10.5463 |
| **0.040** | 2287.00 | 0.5991 | 11.4685 |
| **0.045** | 2462.00 | 0.5861 | 11.8991 |
| **0.050** | 2993.00 | 0.6130 | 13.1197 |
| **0.055** | 3754.00 | 0.6546 | 14.6933 |
| **0.060** | 4947.00 | 0.7194 | 16.8672 |
| **0.065** | 7503.00 | 0.8513 | 20.7725 |

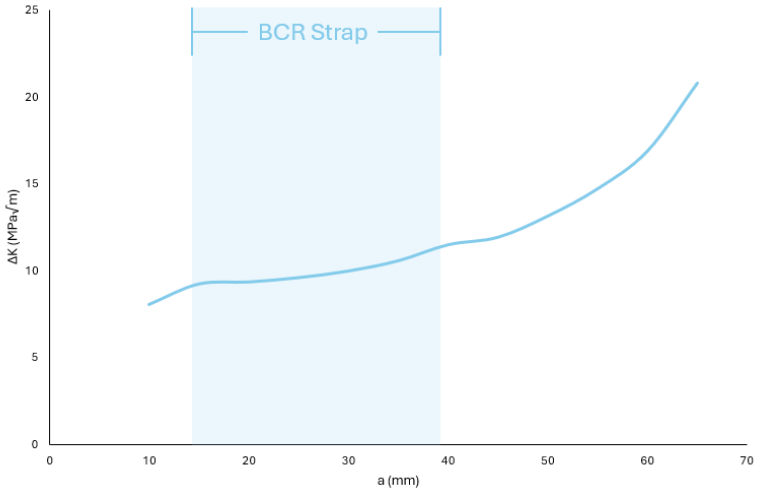


**Figure 16: ΔK for Double Side Symmetric BCRs**

The ΔK trend derived from the SERR values is illustrated in Figure 16. Two spikes are evident at the strap initiation and termination locations. Between these points, the curve flattens, reflecting a reduction in crack-driving force due to the presence of the straps. This behaviour directly demonstrates the retardation effect of the BCRs, which slow crack propagation and consequently extend fatigue life.

The flatter ΔK–a curve within the reinforced region highlights the ability of the straps to redistribute stresses away from the crack tip, delaying crack growth. The retardation effect is strongest within the strap-bonded region, where ΔK remains nearly constant, in contrast to the unreinforced plate where ΔK increases more sharply.

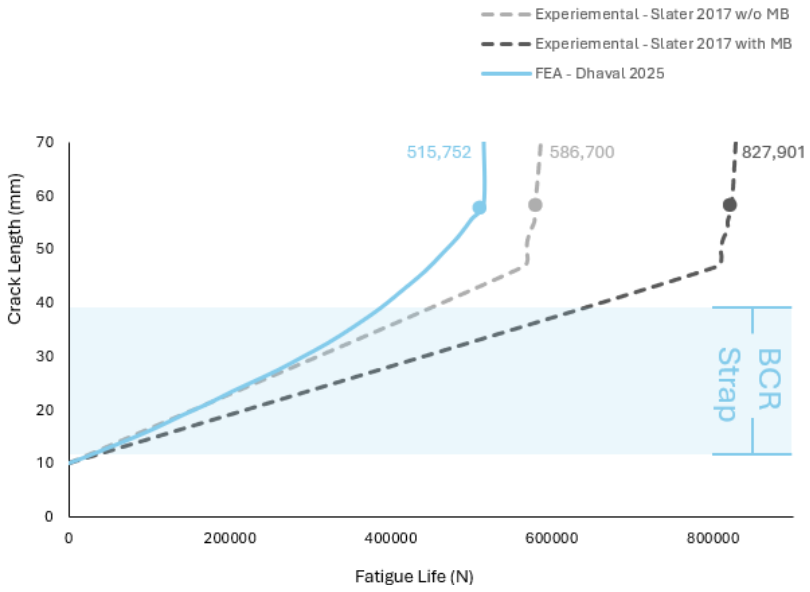


**Figure 17: Fatigue Life for Double Side Symmetric BCRs**

The predicted fatigue life of 515,752 cycles shows strong agreement with Slater's experimental life of 586,700 cycles obtained without marker bands, with a deviation of only ~12%. The experimental case incorporating marker bands (827,901 cycles) produced a significantly longer life; however, this was a result of applying R = 0.8 load ratios during marker-band cycling to assist crack location identification. Such procedures artificially extend life by introducing lower crack-driving conditions in selected regions and are not directly comparable to the baseline fatigue scenario.

**Table 6: Fatigue Life Results for Double Side Symmetric BCRs**

| Model | Fatigue Life | Method | Difference Percentage |
|---|---|---|---|
| **Dhaval 2025** | 515,752 | FEA | - |
| **Slater 2017 w/o MB** | 586,700 | Experimental | 12.2 |
| **Slater 2017 with MB** | 827,901 | Experimental | 60.6 |

When excluding the marker band influence, the FE-predicted results demonstrate excellent correlation with experimental data. The outcome indicates that the modelling methodology not only captures the correct crack retardation effect of symmetric BCRs but also provides a conservative and reliable prediction of fatigue life in reinforced metallic aircraft structures [1][3][23].

### 4.3 Single Side Symmetric BCRs

In addition to the double-side configuration, a single-side symmetric BCR model was analysed to evaluate the effectiveness of reinforcement when applied only to one face of the substrate. This configuration introduces additional complexity due to secondary bending effects and asymmetric load transfer, which have been shown to reduce the efficiency of the reinforcement compared with double-sided cases [1][2][32].

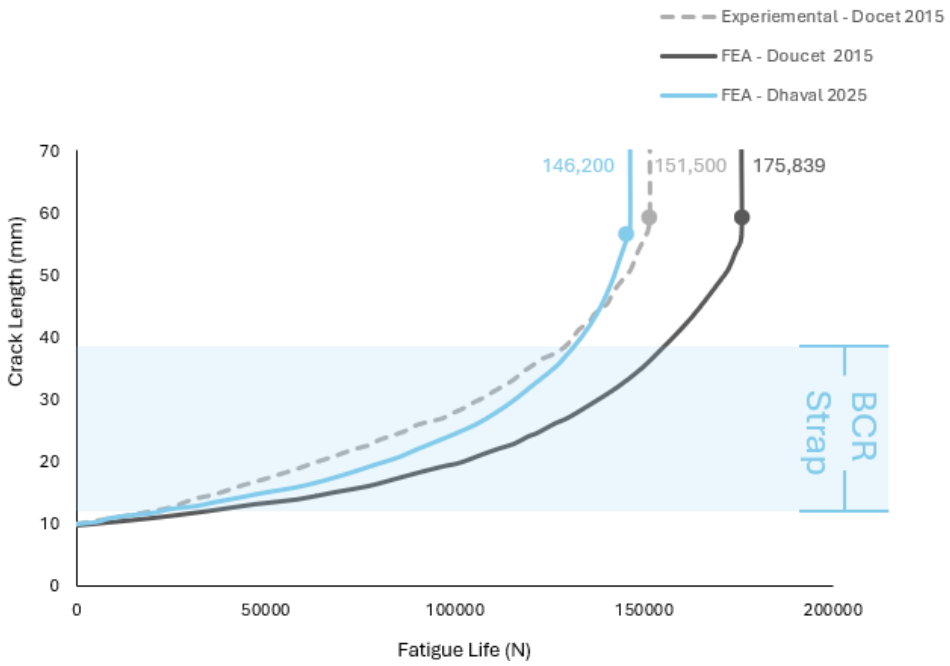


**Figure 18: Fatigue Life for Single Side Symmetric BCRs**

The predicted fatigue life of 146,200 cycles from the present FE model is lower than both Doucet's FEA result (175,839 cycles) and his experimental result (151,500 cycles). This outcome reflects the conservative nature of the present methodology, which incorporated gradual and manual debonding together with consideration of the most critical SERR values at the crack tip. By contrast, Doucet's modelling approach represented debonding through a simplified single node release, and his equivalent SERR values were derived by averaging across both the open and strapped crack surfaces.

**Table 7: Fatigue Life Results for Single Side Symmetric BCRs**

| Model | Fatigue Life | Method | Difference Percentage |
|---|---|---|---|
| **Dhaval 2025** | 146,200 | FEA | - |
| **Doucet 2015** | 151,500 | Experimental | 3.5 |
| **Doucet 2015** | 175,839 | FEA | 20.3 |

The more conservative prediction obtained here is a favourable position, as it ensures that life estimates err on the safe side of experimental results while avoiding the overestimation observed in earlier FEA models.

Overall, the single-side symmetric BCR configuration provides a notable increase in fatigue life compared to the baseline, though its effectiveness is limited relative to the double-sided arrangement. These results are consistent with both experimental and numerical literature, further validating the FE methodology adopted in this study.

### 4.4 Debonding Analysis

An important focus of this study was the modelling of debonding between the adhesive layer and the substrate during crack progression. Earlier finite element studies on bonded crack retarders often did not explicitly incorporate adhesive debonding. Instead, they relied on simplified tie constraints to connect the reinforcement to the substrate [2][32]. While such an approach simplifies modelling, it artificially constrains the adhesive layer, leading to significantly higher predicted fatigue lives as it prevents progressive loss of load transfer at the crack front.

In the present work, a cohesive surface-to-surface interaction was implemented between the substrate and the BCRs, with debonding initiated through a manually defined triangular disbond region. As the crack advanced, the simulation ensured that the condition of the specimen at each stage was carried forward into the subsequent step, allowing for realistic accumulation of adhesive damage. This also aligns with experimental observations in GLARE strap configurations, where disbonding has been identified as a precursor to loss of strap effectiveness [1][23]. The results demonstrate that including gradual disbonding has a significant impact on predicted life. Figure 19 compares fatigue lives predicted with and without manual progressive debonding.

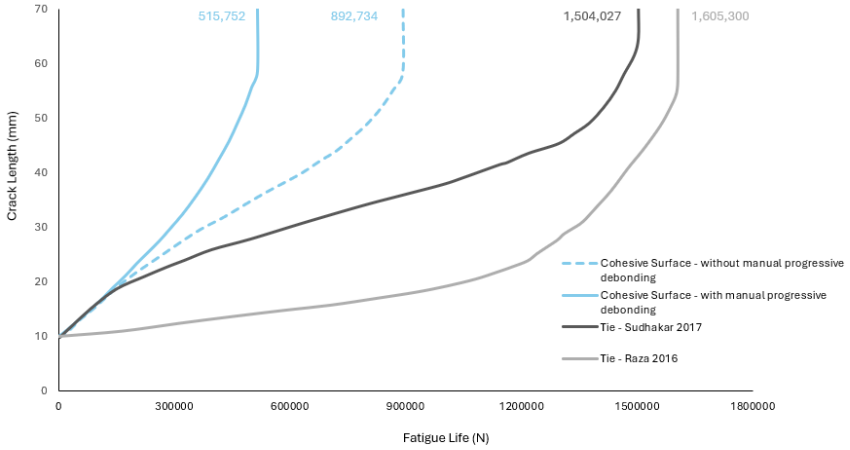


**Figure 19: Fatigue Life using Progressive Debonding vs other FE Modelling methods**

The inclusion of gradual disbonding reduces the effective crack-retardation capability of the straps at longer crack lengths, resulting in earlier onset of accelerated crack growth. The model therefore provides a more conservative and realistic estimate of structural performance than tie-based simulations. Figure 19 shows th comparison of results from the findings of this study compared against the previous studies using Tie connection.

### 4.5 Discussion

While this study has focused on finite element modelling and improving its accuracy, there remain several aspects that could be further refined to enhance predictive fidelity.

One important consideration is the curing process of the adhesive and substrate. The curing cycle can introduce thermal residual stresses, particularly in single-sided BCR configurations where the GLARE strap incorporates both metallic and composite layers. These stresses may influence the fatigue behaviour of the substrate, and their exclusion represents a limitation of the current modelling approach. Incorporating a thermo-mechanical curing step into the FE model would provide a more realistic representation of the initial stress state and potentially improve life predictions.

Another area for improvement concerns the automation of delamination and crack growth simulation. In this study, delamination and crack extension were modelled in increments of 5 mm to make the process manually feasible. A finer step size, such as 1 mm or even 0.5 mm, would have provided a more detailed representation of crack propagation, although at the cost of significant computational effort. Developing automated procedures for incremental crack growth would allow for more granular and accurate fatigue predictions.

Finally, while this work employed multiple simulation steps combined with post-processing of strain energy release rate (SERR) values, it may be possible to achieve a more efficient methodology by implementing a single direct cyclic analysis. Although Abaqus does not natively provide SERR or stress intensity factor outputs for moving cracks in such analyses, this limitation could be overcome by developing a Python-based post-processing routine. For example, contour integral calculations could be automated to extract SERR or $K$.

K values at specified crack lengths. Such an approach would generalise the methodology and allow the fatigue life to be obtained directly from a single Abaqus run, thereby reducing the need for multiple steps and manual calculations.

In summary, while the present methodology has demonstrated good agreement with experimental data, the accuracy and efficiency of the modelling could be further enhanced by incorporating curing-induced residual stresses, refining delamination step sizes, and developing automated tools for direct cyclic fracture analysis.

## 5.0 Conclusion

This study has demonstrated that the application of bonded crack retarders (BCRs) provides a substantial improvement in fatigue performance, extending specimen life by approximately five times relative to unreinforced configurations. Such reinforcement offers clear potential to increase the in-service life of integrated aircraft panels, particularly at critical load-bearing locations where fatigue cracking is most prevalent.

**Table 8: Results Comparison**

| Model | Fatigue Life | Improvement |
|---|---|---|
| **M(T) Specimen Non-Reinforced** | 103,100 | - |
| **Single Sided Symmetric BCRs** | 146,200 | 1.4x |
| **Double Sided Symmetric BCRs** | 515,752 | 5x |

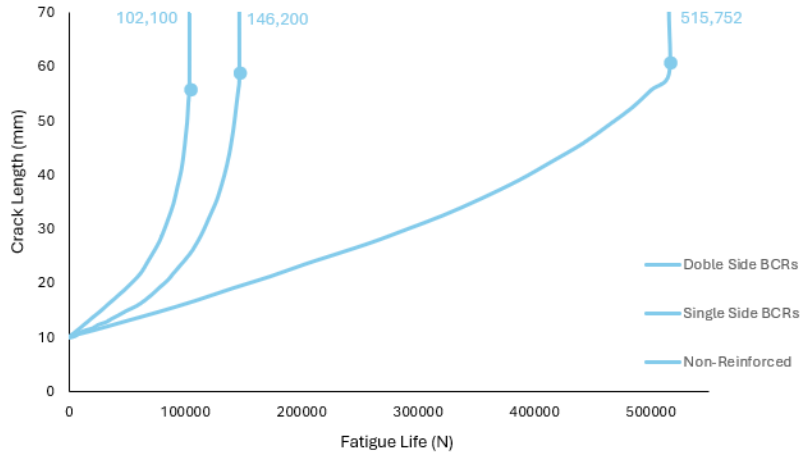


**Figure 20: Fatigue Life Comparison**

The finite element (FE) modelling approach adopted, incorporating Abaqus for fracture mechanics analysis and AFGROW for fatigue life prediction, proved effective in delivering conservative yet reliable life estimates. This methodology has relevance not only for design validation but also for in-service repair scenarios, where bonded reinforcements are employed to restore structural integrity.

A key outcome of this work was the recognition of the importance of accurate interaction modelling. The inclusion of progressive adhesive debonding between the substrate and the reinforcement was shown to significantly improve the predictive accuracy of the FE model. This adjustment ensured that simulation results reflected the physical degradation processes observed experimentally, rather than the artificially extended lives produced by simplified tie connections.

Overall, the study has provided both numerical validation and methodological guidance, reinforcing the role of BCRs as an effective fatigue crack management strategy and confirming the suitability of advanced FE–AFGROW integration for life assessment of metallic aircraft structures.

### 5.1 Future Work

Future work could adopt XFEM-based fatigue crack growth algorithms integrated with VCCT or CZM. Such methods, as demonstrated by Chen et al. [34] and Nikfam et al. [35], allow continuous crack propagation, automatic fracture parameter extraction, and life prediction within a single analysis run. This would enable finer crack growth resolution (≤1 mm), incorporate residual stresses, and eliminate manual iteration, thereby improving both accuracy and efficiency in fatigue life estimation of reinforced aircraft structures.

## III.ACKNOWLEDGEMENTS

I would like to express my sincere gratitude to Cranfield University for granting me the invaluable opportunity to pursue my studies, and for their unwavering support and guidance throughout this academic journey. I extend special thanks to Dr. Wenli Liu for her mentorship, encouragement, and knowledge transfer, which were instrumental to the successful completion of this project. I am profoundly grateful to my parents for their constant belief in me and for shaping me into the person I am today; their encouragement and faith have been my foundation and driving force. Finally, I wish to acknowledge with deep appreciation all those who contributed to the success of this work; their collaboration, effort, and support have been truly invaluable.

## IV.REFERENCES

[1] Doucet, J., Fatigue Life Enhancement of Aircraft Structures through Bonded Crack Retarders, Cranfield University, 2016.

[2] Sudeep, S., A Finite Element Analysis to Study the Effects of Secondary Bending on Aircraft Structures Bonded with Crack Retarders, Cranfield University, 2017.

[3] Slater, D., Bonded Crack Retarders for Fatigue Crack Growth Rate Reduction in Metallic Aircraft Structures, Cranfield University, 2017.

[4] MMPDS, Metallic Materials Properties Development and Standardization, latest applicable edition.

[5] Vlot, A., Gunnink, J. W., Fibre Metal Laminates, An Introduction, Springer, 2001.

[6] Alderliesten, R. C., Benedictus, R., “Fibre metal laminates in aircraft structures”, International Journal of Fatigue, 2008, pp. 1024–1030.

[7] Alderliesten, R. C., Bos, J., Schijve, J., “Fatigue and damage tolerance of GLARE”, Applied Composite Materials, 2003, pp. 65–90.

[8] ABAQUS Documentation, ABAQUS 2024 User’s Guide and Theory Guide, Dassault Systèmes Simulia Corp., 2024.

[9] Zienkiewicz, O. C., Taylor, R. L., The Finite Element Method, McGraw-Hill, 5th ed., 2000.

[10] Anderson, T. L., Fracture Mechanics, Fundamentals and Applications, CRC Press, 3rd ed., 2005.

[11] Broek, D., Elementary Engineering Fracture Mechanics, Springer, 4th ed., 1986.

[12] Tada, H., Paris, P. C., Irwin, G. R., The Stress Analysis of Cracks Handbook, ASME Press, 3rd ed., 2000.

[13] Irwin, G. R., “Analysis of stresses and strains near the end of a crack”, Journal of Applied Mechanics, 1957, pp. 361–364.

[14] Rybicki, E. F., Kanninen, M. F., “A finite element calculation of stress intensity factors by a modified crack closure integral”, Engineering Fracture Mechanics, Vol. 9, 1977, pp. 931–938.

[15] Krueger, R., “The virtual crack closure technique, A critical review”, NASA TM-2002-211628, 2004.

[16] Camanho, P. P., Dávila, C. G., “Mixed-mode decohesion finite elements for the simulation of delamination in composite materials”, NASA TM-2002-211737, 2002.

[17] Turon, A., Camanho, P., Costa, J., Dávila, C., “An engineering solution for mesh size effects in the simulation of delamination using cohesive zone models”, Engineering Fracture Mechanics, Vol. 74, 2007, pp. 1665–1682.

[18] Benzeggagh, M. L., Kenane, M., “Measurement of mixed-mode delamination fracture toughness of unidirectional glass, epoxy composites with mixed-mode bending apparatus”, Composites Science and Technology, Vol. 56, 1996, pp. 439–449.

[19] Reeder, J. R., “3D mixed-mode delamination fracture criteria, an experimentalist’s perspective”, Applied Composite Materials, Vol. 20, 2013, pp. 849–864.

[20] ASTM International, Standard Test Method for Measurement of Fatigue Crack Growth Rates, ASTM E647-15, West Conshohocken, PA, 2015.

[21] Dassault Systèmes, Abaqus Analysis User’s Guide – Virtual Crack Closure Technique Output Variables, 2024.

[22] Barsoum, R. S., “Triangular quarter-point elements as elastic and perfectly-plastic crack tip elements”, International Journal for Numerical Methods in Engineering, Vol. 11, 1977, pp. 85–98.

[23] Jensen, K., Fatigue performance of double-sided GLARE straps on aluminium substrates, Cranfield University, 2016.

[24] ASTM International, Standard Test Method for Linear-Elastic Plane-Strain Fracture Toughness KIC of Metallic Materials, ASTM E399-19, West Conshohocken, PA, 2019.

[25] Newman, J. C., Phillips, E. P., Everett, R. A., “Fatigue crack growth analysis method for aerospace structures – NASGRO methodology”, NASA Technical Memorandum 210837, 2001.

[26] Southwest Research Institute, AFGROW Users Guide and Technical Manual, Version 5.3, 2023.

[27] Slater, D., and Alderliesten, R. C., “Fatigue performance of GLARE and other fibre metal laminates in aircraft structures”, International Journal of Fatigue, Vol. 118, 2019, pp. 1–12.

[28] Suresh, S., Fatigue of Materials, Cambridge University Press, 2nd ed., 1998.

[29] Paris, P. C., Erdogan, F., “A critical analysis of crack propagation laws”, Journal of Basic Engineering, Vol. 85, 1963, pp. 528–534.

[30] Schijve, J., Fatigue of Structures and Materials, Springer, 2nd ed., 2009.

[31] Shakir, S., A comparison of fatigue crack growth performance of two aerospace-grade aluminium alloys reinforced with bonded crack retarders, Coventry University, 2017.

[32] Raza, M. A., Fatigue life enhancement of aluminium panels reinforced with bonded crack retarders, Cranfield University, 2016.

[33] Hill, G., Fatigue performance of aluminium panels reinforced with bonded crack retarders, Cranfield University, 2013.

[34] Chen, Z., Dai, Y., Liu, Y., “Structural fatigue crack propagation simulation and life prediction based on improved XFEM-VCCT,” Engineering Fracture Mechanics, Vol. 310, 2024, 110519.

[35] Nikfam, M. R., Zeinoddini, M., Aghebati, F., Arghaei, A. A., “Experimental and XFEM modelling of high cycle fatigue crack growth in steel welded T-joints,” International Journal of Mechanical Sciences, Vol. 153–154, 2019, pp. 178–193.